Many-valley electron transport in AlGaAs VCSELs

Many-Valley Electron Transport in AlGaAs VCSELs

Marco Calciati[1], Alberto Tibaldi[1], Francesco Bertazzi[1,2], Michele Goano[1,2] and Pierluigi Debernardi[1]

[1] Consiglio Nazionale delle Ricerche (CNR), Istituto di Elettronica e di Ingegneria dell'Informazione e delle Telecomunicazioni (IEIIT), 10129 Turin, Italy
[2] Department of Electronics and Telecommunications, Politecnico di Torino, 10129 Turin, Italy

E-mail: alberto.tibaldi@ieiit.cnr.it

Abstract. Carrier transport in GaAs-based VCSELs is investigated by means of an in-house multiphysics code, with particular emphasis on the description of many-valley effects in the conduction band of AlGaAs barriers. These effects, which are revealed to have a significant impact on the overall VCSEL performance, are accounted for by an effective density of states obtained with a closed-form model. This description has been included in a simplified simulation framework, where most of the DBR pairs are replaced by an equivalent homogeneous layer. This leads to a major reduction of the computational cost, especially important in view of the computer-aided design of 3-D devices.

PACS numbers: 42.55.Px, 72.20.-i, 85.60.Bt

Keywords: VCSELs, AlGaAs, electron transport, optoelectronic device simulation, many-valley semiconductors
Submitted to: *Semicond. Sci. Technol.*

1. Introduction

Vertical-cavity surface-emitting lasers (VCSELs) are among the most interesting semiconductor laser diodes and have become market leaders since several years, covering a range of relevant mass applications, from datacom to sensing in the last generation of smartphones [1]. VCSEL research started in 1979 [2], when for the first time Prof. Kenichi Iga proposed this new kind of lasers. The operation of such complex electro-optical components relies on complex strategies to cope with the sometimes conflicting electrical and optical issues, which therefore require, beside the experimental and technological work, an intense and accurate multiphysics modeling. A representative example of such strong electro-optical interplays can be found in the graded interface distributed Bragg reflectors (DBRs), which consitute the largest part of a VCSEL. In

fact, abrupt GaAs/AlAs layers provide the best DBR reflectivity, but are inadequate from the carrier transport perspective. Fully monolithic InGaAs-GaAs VCSELs incorporating epitaxial distributed Bragg reflectors (DBR) with emission wavelengths of about 960 nm and pulsed threshold currents of 1.3 mA were first demonstrated in 1989 [3]. The dominant limitation of these devices was the high resistance introduced by the p-type GaAs/AlAs DBR mirror. This issue arises from the potential barriers at the heterointerfaces, which are also the main cause of self-heating in VCSELs. In the early '90s, several solutions such as modulation doping [4] or AlGaAs intermediate layers [5,6] were proposed. These approaches were not decisive, since they were temperature-dependent or did not provide an adequate reduction of the series resistance.

An effective solution, still adopted today, was the introduction of graded interfaces, proposed in [7] and [8], where composition grading was achieved by means of a superlattice, grown with molecular beam epitaxy (MBE). A continuous Al composition grading was later obtained by different techniques such as phase-locked epitaxy (PLE) [9], metal-organic chemical vapor deposition (MOCVD) [10, 11] or MBE [12]. In order to illustrate the benefits of graded interfaces, Fig. 1 compares the light-current-voltage (LIV) characteristics of three typical VCSEL structures (for details see Section 3) featuring abrupt and linearly graded interfaces with thicknesses of 10 nm and 20 nm. One can observe that the VCSEL with interfaces does not reach lasing operation. The modification of the interfaces leads to a twofold effect, both optical and electrical. In fact, a graded DBR results in a lower reflectivity [13], which corresponds to a higher threshold (threshold gain is 765, 915 and 1393 cm^{-1} for the abrupt, 10 nm and 20 nm

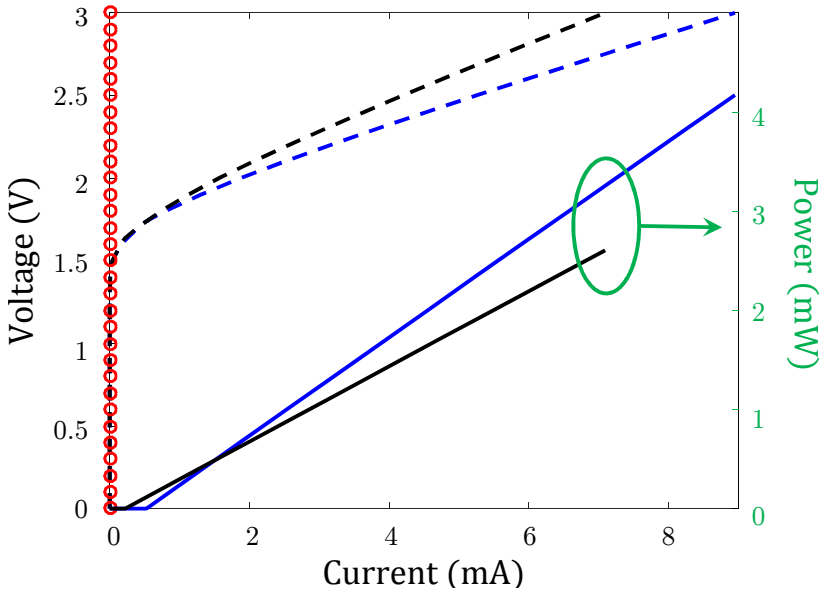

Figure 1. Simulated LIV characteristics (for structure detail see Section 3 and related text) for three VCSELs with abrupt (red lines) and graded interfaces with thicknesses of 10 nm (black lines) and 20 nm (blue lines). Dashed and solid curves refer to IV and IL characteristics.

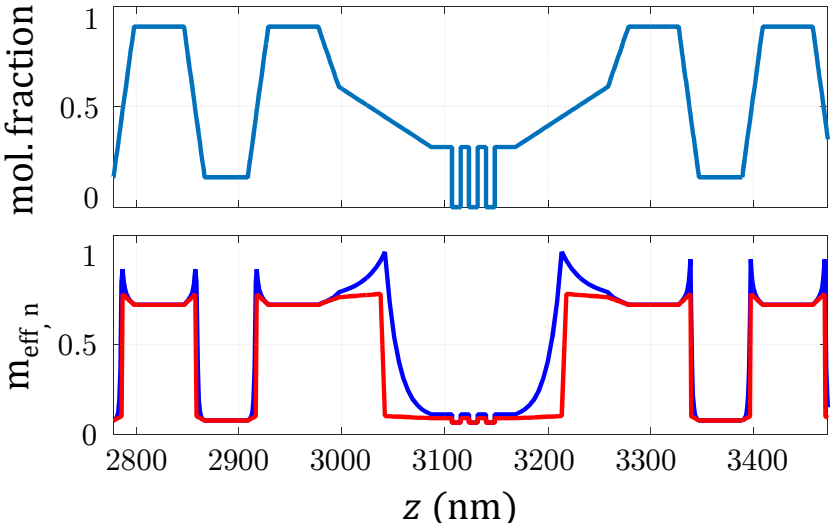

Figure 2. Molar fraction (top) and DoS electron effective mass (bottom) with the single-valley (red line) and many-valley models (Boltzmann approximation, blue line); $z = 0$ corresponds to the outcoupling p-side facet (see also Fig. 6).

cases respectively), but also to a higher output coupling efficiency. This is shown by the higher slope of the blue LI curve, which corresponds also to a higher current flow.

As suggested by this example, the interplay between different physical phenomena makes the VCSEL design a complex task. For this reason, the experimental activity has been always supported by a strong theoretical counterpart [14–17]. Focusing on electron transport, a remarkable work has been published by David Winston, who developed the free 1-D software SimWindows [18]. Nowadays, comprehensive simulators are still essential tools to explore the design parameter space for an optimum design while keeping at bay the cost factor and the time required for a design cycle. At present, the most advanced published model is reported in [19], on which was based the VCSEL simulator (presently no longer supported) in Synopsys TCAD Sentaurus.

In this work AlGaAs-based VCSELs are investigated, with a special focus on many-valley electron conduction properties. The study is carried out with our in-house Drift-dIffusion ANAlysis code (DIANA). This is based on the numerical solution of the Poisson and continuity equations by means of a generalized Newton method, where the current densities are approximated by means of the Scharfetter-Gummel (SG) relation [20]. Even if a drift-diffusion model may sound as old-fashioned, for CAD-level tools it is the only approach compatible with the large size and considerable complexity of VCSEL structures.

Modeling these optoelectronic devices requires to deal with high carrier concentrations, leading to regions where the semiconductor is degenerate. In this view, it is necessary to use Fermi-Dirac statistics to describe the carrier distribution, whose effect is included by additional terms in the SG potential. A similar idea is applied to the heterointerfaces, with the relevant composition-dependent corrections. Incomplete

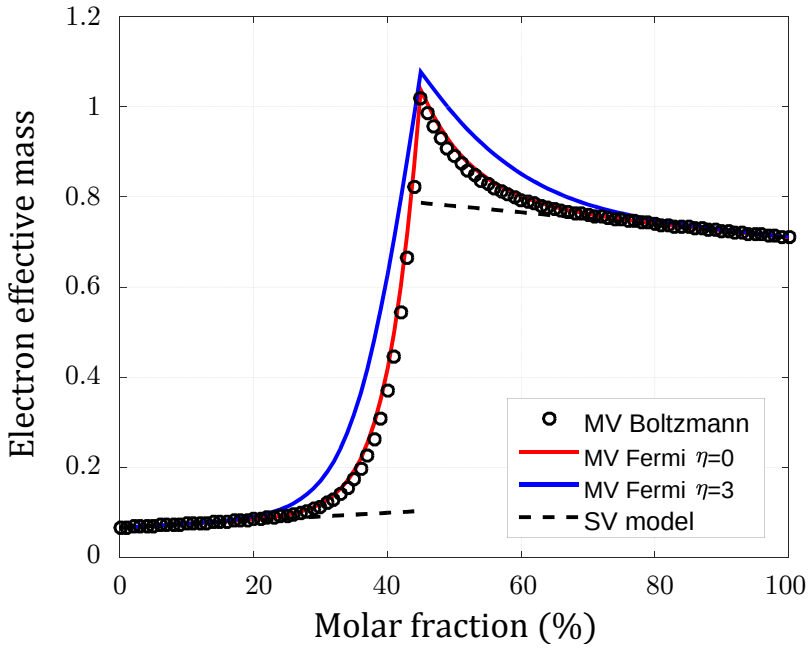

Figure 3. Effective DoS electron mass vs. molar fraction in a $Al_xGa_{1-x}As$ alloy for the different models discussed in the paper.

ionization is also accounted for, being especially relevant in AlGaAs systems. In addition to the "standard" Shockley-Read-Hall, radiative and Auger recombination processes, the key objective of a VCSEL simulator is to compute the optical emission power from stimulated recombination. To this aim, VELM, an efficient electromagnetic simulator, is used to estimate the lasing wavelength and threshold gains [21]. The photon rate equation that balances the material gain and the device losses is coupled to the drift-diffusion model through the stimulated recombination term (see *e.g.* Chap. 3 in [1]).

2. Many-valley model

The conduction band structure of the $Al_xGa_{1-x}As$ system deserves particular attention when a VCSEL is electrically pumped through its mirrors. In fact, from Table 1, in the neighborhood of the critical molar fraction $x = 0.45$ the Γ and X conduction valleys display the same energy gap. Beyond this value, the semiconductor becomes indirect. In a single valley (SV) perspective [22], the density of states (DoS) electron mass exhibits a sharp discontinuity at $x = 0.45$, as can be seen in Fig. 3. Due to the graded heterointerfaces, usually present both in the DBRs and in the cavity region (see Fig. 2), the molar fraction crosses the critical value in several sections, so that the SV approach might lead to inaccurate results. In the following a more realistic many-valley (MV) approach is compared to the standard SV model. The present MV approach can be easily implemented also in commercial codes. Accounting for the complete electron band structure of an AlGaAs alloy requires to compute the electron density as the sum

of 3 contributions‡ corresponding to the Γ, X and L minima [31], [32]:

$$n_{\mathrm{tot}} = N_{\mathrm{C,eff}}\,\mathcal{F}_{1/2}(\eta_x) = \begin{cases} n_\Gamma \left(1 + \dfrac{n_\mathrm{X}}{n_\Gamma} + \dfrac{n_\mathrm{L}}{n_\Gamma}\right) & x < 0.45 \\ \\ n_\mathrm{X} \left(1 + \dfrac{n_\Gamma}{n_\mathrm{X}} + \dfrac{n_\mathrm{L}}{n_\mathrm{X}}\right) & x \geq 0.45, \end{cases} \tag{1}$$

where $n_j = N_{\mathrm{C}j}\,\mathcal{F}_{1/2}(\eta_j)$, being $\mathcal{F}_{1/2}$ the Fermi-Dirac integral of order 1/2, which can be approximated by an exponential function for non-degenerate operation [33, 34]. The argument $\eta_j = (E_{\mathrm{F},n} - E_j)/(k_\mathrm{B}T)$ is the distance of the quasi-Fermi level $E_{\mathrm{F},n}$ from the minimum of valley $j = \{\mathrm{X}, \mathrm{L}, \Gamma\}$; $k_\mathrm{B}T$ is the temperature equivalent energy. Depending on the molar fraction, η_x in Equation (1) is equal to η_Γ or η_X. The density of states $N_{\mathrm{C}j}$ is given by the textbook formula:

$$N_{\mathrm{C}j} = 2\left(\frac{2\pi m_0 k_\mathrm{B} T}{h^2}\right)^{\frac{3}{2}} m_j^{\frac{3}{2}}. \tag{2}$$

When the Boltzmann approximation holds, the $E_{\mathrm{F},n}$ terms in the exponentials of Equation (1) cancel out and an analytic expression for the effective electron mass is obtained, which does not depend on the electron density

$$m_{\mathrm{eff}} = \begin{cases} m_\Gamma \left[1 + \left(\dfrac{m_\mathrm{L}}{m_\Gamma}\right)^{\frac{3}{2}} \mathrm{e}^{-\Delta_{\mathrm{L}\Gamma}} + \left(\dfrac{m_\mathrm{X}}{m_\Gamma}\right)^{\frac{3}{2}} \mathrm{e}^{-\Delta_{\mathrm{X}\Gamma}}\right]^{\frac{2}{3}} & x < 0.45 \\ \\ m_\mathrm{X} \left[1 + \left(\dfrac{m_\mathrm{L}}{m_\mathrm{X}}\right)^{\frac{3}{2}} \mathrm{e}^{-\Delta_{\mathrm{LX}}} + \left(\dfrac{m_\Gamma}{m_\mathrm{X}}\right)^{\frac{3}{2}} \mathrm{e}^{+\Delta_{\mathrm{X}\Gamma}}\right]^{\frac{2}{3}} & x \geq 0.45, \end{cases} \tag{3}$$

where $\Delta_{ij} = (E_{\mathrm{g}i} - E_{\mathrm{g}j})/(k_\mathrm{B}T)$. Substituting Equation (3) in Equation (2) leads to the effective DoS $N_{\mathrm{C,eff}}$ that, inserted in Equation (1), provides the many-valley total electron population.

3. Numerical results

The device investigated in the following is based on the AlGaAs VCSEL described in [38]. It consists of 39.5 n-doped bottom mirror pairs, three GaAs quantum wells inside a one-wavelength thick cavity, and 23 p-doped top mirror pairs. For simplicity, dopings in the DBRs are assumed constant ($3 \times 10^{18}\,\mathrm{cm}^{-3}$ for the p-DBR and $2 \times 10^{18}\,\mathrm{cm}^{-3}$ for the n-DBR). The molar composition of the central region (cavity and first mirror pairs aside) of the VCSEL is shown in Fig. 2. The set of parameters used in the drift-diffusion simulations is reported in Table 1; for the meaning of the parameters not defined in this paper, see [39].

‡ Band mixing of zone-center Γ and zone-edge X states is not considered here, as mixing effects are expected to be important only in highly confined nanostructures such as short period GaAs/AlAs superlattices [23–28] and quantum dots [29, 30].

Table 1. Material parameters of AlGaAs used in the present simulations.

Parameter	$Al_xGa_{1-x}As$	Ref.
$E_{g,\Gamma}$ (eV)	$1.424 + 1.247x$	[31]
$E_{g,X}$ (eV)	$1.900 + 0.125x + 0.143x^2$	[31]
$E_{g,L}$ (eV)	$1.708 + 0.642x$	[31]
m_Γ	$0.067 + 0.083x$	[35]
m_X	$0.850 - 0.140x$	[35]
m_L	$0.560 + 0.100x$	[35]
ϵ	$12.90 - 2.84x$	[36]
$\mu_{n,\Gamma}$ ($cm^2/s/V$)	$8000 - 22000x + 10000x^2$	[37]
$\mu_{n,X}$ ($cm^2/s/V$)	$-255 + 1160x - 720x^2$	[37]
μ_p ($cm^2/s/V$)	$400 - 700x + 450x^2$	[37]
χ_Γ (eV)	$4.07 - 0.7482x$	[37]
χ_X (eV)	$3.594 + 0.3738x - 0.143x^2$	[37]
ΔE_A (eV)	0.026	[31]
ΔE_D (eV)	0.005	[31]
τ_n (s)	5×10^{-9}	[36]
τ_p (s)	20×10^{-9}	[36]
B (cm^3/s)	1.8×10^{-10}	[31]
C_n (cm^6/s)	1.2×10^{-31}	[36]
C_p (cm^6/s)	8.5×10^{-31}	[36]

In Fig. 3 the MV DoS electron mass is shown as a function of the alloy molar fraction. The unphysical DoS discontinuity is removed and a maximum mass is achieved at the critical molar fraction, which reflects the fact that a balanced contribution from all three valleys occurs in that molar region. The effect of high carrier densities is also investigated by considering as an example the DoS effective mass in the degenerate case with $\eta = 3$. However, up to $\eta = 0$, the analytic formula Equation (3) based on Boltzmann statistics is accurate and proves to be a very good approximation for standard VCSEL operation. In fact, the LIV curves (see *e.g.* Fig. 4) are almost unchanged by using the Fermi DoS effective mass (upgraded after every voltage step) or the Boltzmann one, which does not depend on voltage.

In the lower part of Fig. 2 the longitudinal DoS effective mass profile is shown for the central part of the VCSEL under analysis and the SV and MV approaches are compared. The overall impact of the MV approach is shown in Fig. 4, where the LIV curves are computed by means of DIANA. The present investigation is concerned with an inherently longitudinal transport effect; therefore a simplified 1-D version of the code is used, for which the transverse details are not needed. It can be clearly seen that the SV approach leads to currents lower by about 25%, due to the underestimated carrier densities of the SV approach. These are shown in Fig. 5 for the same longitudinal section of Fig. 2); in particular, the largest carrier density deviations occur in the cavity, in correspondence of the gradings next to the active region.

In view of the more demanding task of performing the comprehensive simulation

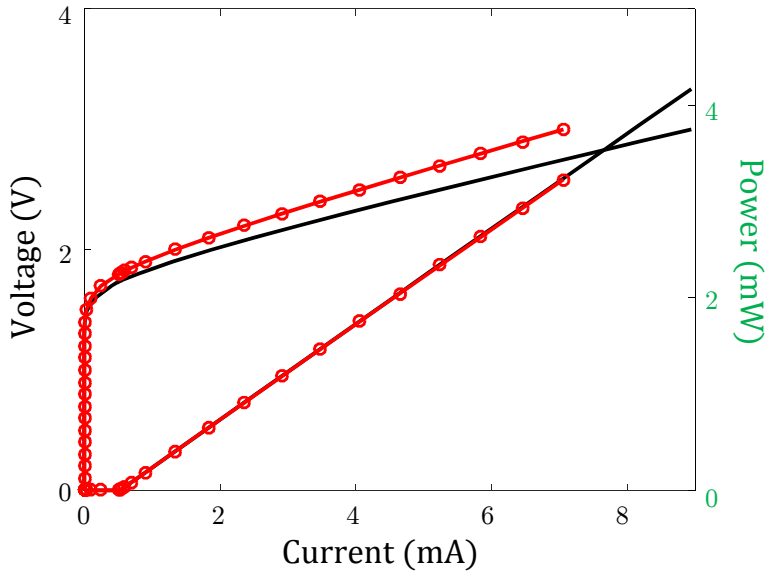

Figure 4. Comparison of the LIV characteristics computed with SV (red lines) or MV (black lines) approaches.

of 3-D axisymmetric circular devices, the electrical structure can be simplified leading to a considerable reduction of the system unknowns. This has been proposed in [19] and implemented in several commercial codes (*e.g.* Synopsys TCAD Sentaurus and Crosslight PICS3D). In order to investigate this strategy, the DBR pairs far from the active region are substituted with a uniform material, whose molar fraction is determined

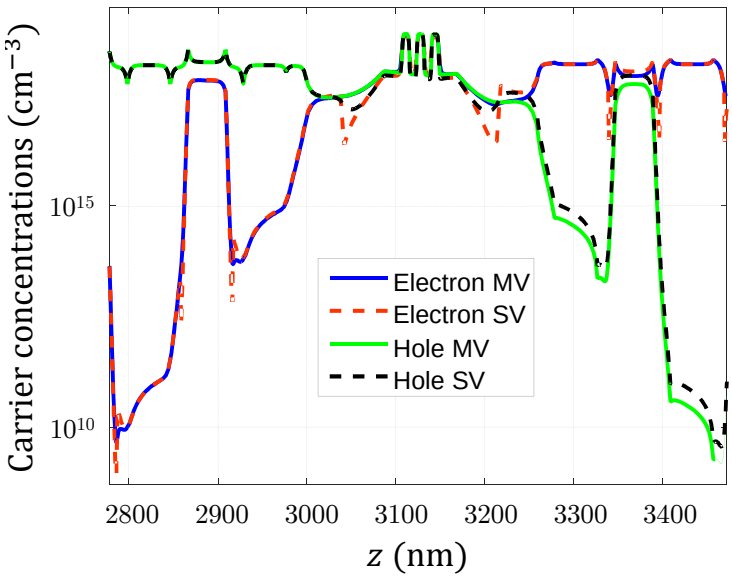

Figure 5. Carrier concentration profiles at 1.8V for in the central part of the VCSEL, comparing the SV and MV models.

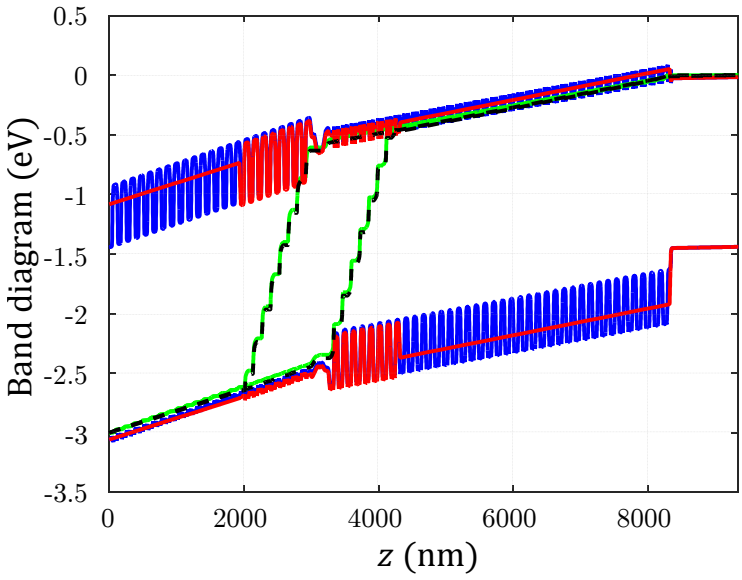

Figure 6. VCSEL band diagram (blue lines or by using an equivalent layer whose molar fraction set to 0.441, red lines) and quasi-Fermi levels (green lines for the complete case, black dashed lines for the equivalent layer case).

in such a way to achieve the same electrical characteristics of the actual device [40]. As an example, Fig. 6 shows the band diagram of the original and simplified structures for a molar fraction of the equivalent layer of 0.441. It can be seen that the agreement is excellent. Fig. 7 compares the IV curves for the full VCSEL structure (black circles) and of the simplified layout (blue line). To provide additional information, the green and red curves show the IV curves obtained with $x = 0.4$ and $x = 0.5$ for the equivalent layer. The optimal $x = 0.441$ value is achieved by minimizing the difference between the full and equivalent IV responses. It can be observed that this value is lower than the average alloy composition of the DBRs (0.15 and 0.9, *i.e.* 0.525).

4. Conclusions

We have applied our new in-house drift-diffusion code, written with a special attention to AlGaAs-based VCSELs, to investigate the effects of many-valley electron transport on a typical VCSEL, electrically pumped through the DBRs. Simulations predict a current increase of about 25% using the more realistic MV transport model, which can be introduced by using an effective DoS electron mass. The effectiveness of this MV description has been also demonstrated within a strategy aimed at defining a simplified equivalent geometry where several DBR pairs are replaced by a uniform effective material. This is the first step towards a comprehensive electro-thermo-optical simulator, which will be addressed in future works.

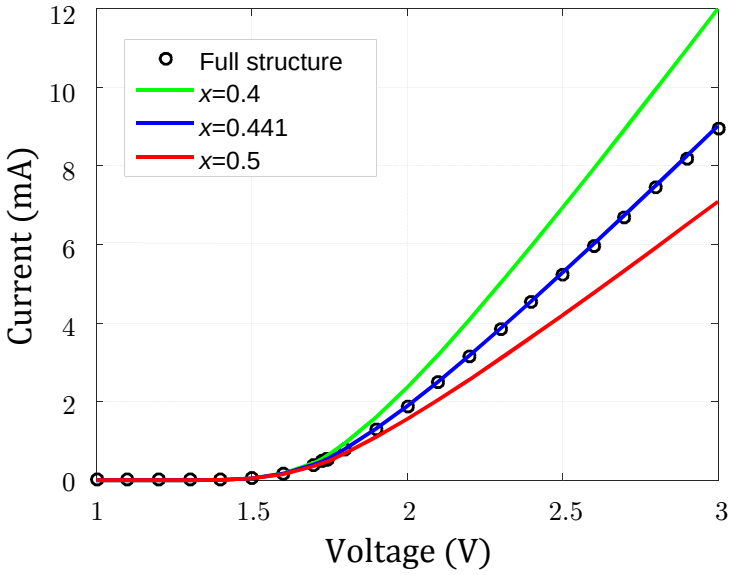

Figure 7. IV curve of the full VCSEL structure (open circles) compared with those obtained by the effective layer approach for different molar fractions (solid lines).

References

[1] Michalzik R, ed 2013 *VCSELs: Fundamentals, Technology and Applications of Vertical-Cavity Surface-Emitting Lasers* (Berlin: Springer-Verlag)

[2] Soda H, Iga K I, Kitahara C and Suematsu Y 1979 GaInAsP/InP surface emitting injection lasers *Japan. J. Appl. Phys.* **18**(12) 2329

[3] Jewell J L, Lee Y H, Walker S, Scherer A, Harbison J P, Florez L T and L M S 1989 Low-threshold electrically pumped vertical-cavity surface-emitting microlasers *Electron. Lett.* **25** 1123–1124

[4] Schubert E F, Tu L W, Zydzik G J, Kopf R F, Benvenuti A and Pinto M R 1992 Elimination of heterojunction band discontinuities by modulation doping *Appl. Phys. Lett.* **60**(4) 466–468

[5] Lee Y H, Tell B, Brown-Goebeler K, Jewell J L and Hove J V 1990 Top-surface-emitting GaAs four-quantum-well lasers emitting at 0.85 μm *Electron. Lett.* **26**(11) 710–711

[6] Tell B, Lee Y H, Brown-Goebeler K F, Jewell J L, Leibenguth R E, Asom M T, Livescu G, Luther L and Mattera V D 1990 High-power cw vertical-cavity top surface-emitting GaAs quantum well lasers *Appl. Phys. Lett.* **57**(18) 1855–1857

[7] Geels R S, Corzine S W, Scott J W, Young D B and Coldren L A 1990 Low threshold planarized vertical-cavity surface-emitting lasers *IEEE Photon. Technol. Lett.* **2**(4) 234–236

[8] Tai K, Yang L, Wang Y H, Wynn J D and Cho A Y 1990 Drastic reduction of series resistance in doped semiconductor distributed Bragg reflectors for surface-emitting lasers *Appl. Phys. Lett.* **56**(25) 2496–2498

[9] Walker J D, Kuchta D M and Smith J S 1991 Vertical-cavity surface-emitting laser diodes fabricated by phase-locked epitaxy *Appl. Phys. Lett.* **59**(17) 2079–2081

[10] Zhou P, Cheng J, Schaus C F, Sun S Z, Zheng K, Armour E, Hains C, Hsin W, Myers D R and Vawter G A 1991 Low series resistance high-efficiency GaAs/AlGaAs vertical-cavity surface-emitting lasers with continuously graded mirrors grown by MOCVD *IEEE Photon. Technol. Lett.* **3**(7) 591–593

[11] Lear K L, Schneider R P, Choquette K D, Kilcoyne S P, Figiel J J and Zolper J C 1994 Vertical cavity surface emitting lasers with 21% efficiency by metalorganic vapor phase epitaxy *IEEE Photon. Technol. Lett.* **6**(9) 1053–1055

[12] Chalmers S A, Lear K L and Killeen K P 1993 Low resistance wavelength-reproducible p-type (Al,Ga)As distributed Bragg reflectors grown by molecular beam epitaxy *Appl. Phys. Lett.* **62**(14) 1585–1587
[13] Debernardi P and Orta R 2007 Analytical electromagnetic solution for Bragg mirrors with graded interfaces and guidelines for enhanced reflectivity *IEEE J. Quantum Electron.* **43**(3) 269–274
[14] Hasnain G, Tai K, Yang L, Wang Y H, Fischer R J, Wynn J D, Weir B, Dutta N K and Cho A Y 1991 Performance of gain-guided surface emitting lasers with semiconductor distributed Bragg reflectors *IEEE J. Quantum Electron.* **27**(6) 1377–1385
[15] Geels R S, Corzine S W and Coldren L A 1991 InGaAs vertical-cavity surface-emitting lasers *IEEE J. Quantum Electron.* **27**(6) 1359–1367
[16] Zeeb E and Ebeling K J 1992 Potential barriers and current-voltage characteristics of p-doped graded AlAs/GaAs heterojunctions *J. Appl. Phys.* **72**(3) 993–999
[17] Michalzik R and Ebeling K J 1993 Modeling and design of proton-implanted ultralow-threshold vertical-cavity laser diodes *IEEE J. Quantum Electron.* **29**(6) 1963–1974
[18] Winston D W and Hayes R E 1998 Optoelectronic device simulation of Bragg reflectors and their influence on surface-emitting laser characteristics *IEEE J. Quantum Electron.* **34**(4) 707–715
[19] Streiff M, Witzig A, Pfeiffer M, Royo P and Fichtner W 2003 A comprehensive VCSEL device simulator *IEEE J. Select. Topics Quantum Electron.* **9**(3) 879–891
[20] Selberherr S 1984 *Analysis and Simulation of Semiconductor Devices* (Wien: Springer-Verlag)
[21] Tibaldi A, Debernardi P and Orta R 2015 High-contrast grating performance issues in tunable VCSELs *IEEE J. Quantum Electron.* **51**(12) 2400407
[22] Adachi S, ed 1993 *Properties of Aluminium Gallium Arsenide* EMIS Datareviews Series (London: INSPEC)
[23] Sham L J and Lu Y T 1989 Theory of electronic structure in superlattices *J. Lumin.* **44**(4) 207–221
[24] Holtz M, Cingolani R, Reimann K, Muralidharan R, Syassen K and Ploog K 1990 Electronic structure of GaAs/AlAs symmetric superlattices: A high-pressure study near the type-I–type-II crossover *Phys. Rev. B* **41** 3641–3646
[25] Nakayama M, Imazawa K, Tanaka I and Nishimura H 1993 Γ-X mixing effects on photoluminescence intensity in GaAs/AlAs type-II superlattices *Solid State Commun.* **88**(1) 43–46
[26] Ivchenko E L, Kiselev A A, Fu Y and Willander M 1994 Valley mixing effects on electron tunneling transmission in GaAs/AlAs heterostructures *Solid-State Electron.* **37**(4) 813–816
[27] Voliotis V, Grousson R, Lavallard P, Ivchenko E L, Kiselev A A and Planel R 1994 Absorption coefficient in type-II GaAs/AlAs short-period superlattices *Phys. Rev. B* **49** 2576–2584
[28] Wang L W and Zunger A 1997 Magnitude and size scaling of intervalley coupling in semiconductor alloys and superlattices *Phys. Rev. B* **56** 12395–12403
[29] Li G H, Goñi A R, Syassen K, Brandt O and Ploog K 1995 High pressure study of Γ-X mixing in InAs/GaAs quantum dots *J. Phys. Chem. Solids* **56**(3) 385–388
[30] Wang L W, Franceschetti A and Zunger A 1997 Million-atom pseudopotential calculation of γ-X mixing in GaAs/AlAs superlattices and quantum dots *Phys. Rev. Lett.* **78**(14) 2819–2822
[31] Casey Jr H C and Panish M B 1978 *Heterostructure Lasers. Part A: Fundamental Principles* (New York: Academic Press)
[32] Vahanyan A I 1982 On the determination of some parameters of the band structure of the many-valley semiconductors *Sov. Phys. – Semicond.* **16**(3) 520–523
[33] Goano M 1993 Series expansion of the Fermi-Dirac integral $\mathcal{F}_j(x)$ over the entire domain of real j and x *Solid-State Electron.* **36**(2) 217–221
[34] Goano M 1995 Algorithm 745. Computation of the complete and incomplete Fermi-Dirac integral *ACM Trans. Math. Software* **21**(3) 221–232
[35] Adachi S 1985 GaAs, AlAs, and $Al_xGa_{1-x}As$: Material parameters for use in research and device applications *J. Appl. Phys.* **58**(3) R1–R29
[36] Ioffe Physico-Technical Institute Physical properties of semiconductors `http://www.ioffe.ru/`

SVA/NSM/Semicond/index.html URL http://www.ioffe.ru/SVA/NSM/Semicond/index.html

[37] Shur M 1990 *Physics of Semiconductor Devices* (Englewood Cliffs, NJ: Prentice-Hall)

[38] Debernardi P, Kroner A, Rinaldi F and Michalzik R 2009 Surface relief versus standard VCSELs: A comparison between experimental and hot-cavity model results *IEEE J. Select. Topics Quantum Electron.* **15**(3) 828–837

[39] Calciati M, Goano M, Bertazzi F, Vallone M, Zhou X, Ghione G, Meneghini M, Meneghesso G, Zanoni E, Bellotti E, Verzellesi G, Zhu D and Humphreys C 2014 Correlating electroluminescence characterization and physics-based models of InGaN/GaN LEDs: Pitfalls and open issues *AIP Adv.* **4**(6) 067118

[40] Calciati M, Debernardi P, Goano M and Bertazzi F 2015 Towards a comprehensive 3D VCSEL model: Electrical simulations with PICS3D in *2015 Fotonica AEIT Italian Conference on Photonics Technologies* (Torino, Italy)